Pygmy and giant dipole resonances in the nitrogen isotopes

Hai-Liang Ma,[1,*] Bao-Guo Dong,[1] Yu-Liang Yan,[1] Huan-Qiao Zhang,[1] Da-Qing Yuan,[1] Shen-Yun Zhu,[1] and Xi-Zhen Zhang[1]
[1]*Department of Nuclear Physics, China Institute of Atomic Energy, Post Office Box 275(18), Beijing 102413, China*
(Received 15 July 2015; revised manuscript received 25 November 2015; published 25 January 2016)

The configuration-interaction shell model with the WBP10 effective interaction has been used to investigate the pygmy and giant dipole resonances in the nitrogen isotopes. Large enhancement of low-lying dipole strength, i.e., pygmy dipole resonances (PDRs), is predicted in the neutron-rich ^{17,18,19,20}N. The nature of the PDRs is analyzed via the transition densities and transition matrix elements. It turns out these PDRs involve a larger amount of excitations between the $2s1d$ and loosely bound $1f2p$ shells. Combining with the transition densities, it is concluded that the PDRs in ^{17,18,19,20}N are collective and due to the oscillation between the excess neutrons and the isospin saturated core. The isospin dependence of energy splitting and sum rule of isospin doublets is discussed. The theoretical energy splitting of isospin doublets can significantly deviate from the systematic values when nucleus is far away from the β-stability line. The ratios of $T_<$ and $T_>$ energy-weighted sum rule (EWSR) are consistently larger than the systematic values, and it is noticed that the calculated EWSR ratio over the systematic ratio increases with increasing isospin almost linearly. We also calculated the photoabsorption cross sections for the nitrogen isotopes. We proposed the normalization factors for 0–1$\hbar\omega$ and 2–3$\hbar\omega$ calculations. After the normalization, the shell model has well reproduced the experimental photoabsorption cross sections in ^{14,15}N, especially the detailed structure of resonances.

DOI: 10.1103/PhysRevC.93.014317

I. INTRODUCTION

Isovector giant dipole resonance (GDR) is the most well-established collective oscillating mode throughout the mass table with large photoabsorption cross sections [1], exhausting most of the classical Thomas-Reich-Kuhn (TRK) sum rule [2,3]. Microscopically the GDR is described as a coherent superposition of particle-hole excitations resulting from the action of an electromagnetic operator on the nuclear ground state [4]. Another kind of electric dipole excitation with collective characteristics can be developed in nuclei with large neutron-proton excess; i.e., the less tightly bound nucleons can oscillate against the isospin saturated core [5–8]. This soft mode will result in a large enhancement of electric dipole response in the low-energy region, which exhausts only a few percent of the total energy-weighted sum rule (EWSR), hence named the pygmy dipole resonance (PDR). The significance of the PDRs is that not only do they provide a novel collective behavior in nuclear structure but also nucleon capture rates could be largely enhanced in the astrophysical r-process nucleosynthesis [9].

The PDRs in neutron-rich heavy and medium-heavy nuclei have been intensely studied by various approaches; see Ref. [7] for a review. The most widely used microscopical approaches are based on the relativistic and nonrelativistic mean-field or density functional theories plus (quasiparticle-)random-phase-approximation (RPA) [10–18]. Some of the calculations have also incorporated the phonon coupling [19] or the continuum states [20]. However, the collectivity of PDRs is still much debated. In heavy nuclei, the PDRs are predicted to be collective and due to the vibration of the excess neutrons against the inert isospin saturated core [21]. In light nuclei, not only can PDRs be developed by the collective soft mode [5,6], but also the fragmentation of the GDRs can shift the dipole strength to lower energies [21–23]. Relativistic and nonrelativistic theories have predicted these low-lying strengths to be of noncollective nature [19,21,24]. Moreover, the single-particle excitations near the threshold can enhance the dipole excitations [11,25,26]. The observed dipole strength at very low excitation energies for the one-neutron halo nuclei ^{11}Be [27] and ^{19}C [28] was interpreted as this threshold effect.

In light nuclei, another option to study the isovector dipole resonances is using the configuration-interaction shell model (SM) [29–31]. Decades ago it was already realized that "the gross structure of photo absorption curves in light nuclei (position and width of the main maximum, configurational and isospin splitting) can be well understood on the basis of the shell model if one takes into account the residual interaction between the nucleons" [29]. The configuration interaction is not included in the most widely used mean-field plus RPA approaches. However, it was shown that the phonon coupling, which can be seen as including the minimal configuration interaction in the mean-field-based theories, is crucial to obtain a reasonable result of PDRs in the study of neutron-rich oxygen isotopes [19]. It is convenient to take into account of multiple particle-hole excitations and configuration interactions in the shell model. For example, the PDRs in neutron-rich oxygen isotopes were predicted by the shell model [30] and then confirmed experimentally [22]. In order to get insight into the collectivity of the PDRs, authors in Ref. [23] have combined the shell-model transition densities and matrix elements, showing that the PDR in ^{17}Ne is collective and due to the oscillation of the valence protons against the interior core, while in ^{18}Ne the dipole resonance in the PDR region is noncollective and more likely to be the configuration splitting of the giant dipole resonances.

For an entire nuclear chain, it is also interesting to investigate the isospin dependence of electric dipole strength

*mhl624@ciae.ac.cn

as well as photoabsorption cross sections approaching the neutron drip line. The PDRs in some light-mass even-Z nuclei, such as oxygen and carbon isotopes, have already been studied by the shell model in Refs. [30,31].

In this paper, the electric dipole strengths and photoabsorption cross sections in the odd-Z nitrogen isotopes are investigated by the shell model in the $spsdpf$ space with the WBP10 interaction [32]. The details of the calculation are given in Sec. II. In Sec. III, we give the neutron and proton separation energies for the entire nitrogen chain to check the appropriateness of the WBP10 interaction. The single-particle wave functions are checked by comparing the theoretical mass radius with the experimental values. Then the strengths of dipole responses in $^{14-20}$N are discussed in Sec. IV. The enhanced pygmy dipole resonances in the neutron-rich nitrogen isotopes are analyzed by looking into the transition densities and matrix elements. In Sec. V, the isospin dependence of sum rule and energy splitting for isospin doublets are discussed. The systematics of the PDRs in the odd-Z nitrogen isotopes are compared with the even-Z carbon and oxygen isotopes in Sec. VI. In Sec. VII, we give the photoabsorption cross sections in the nitrogen isotopes. Finally a summary will be given in Sec. VIII.

II. CALCULATION DETAILS

In our shell-model calculations, the NUSHELL@MSU code [33] with the effective interaction WBP10 [32] in the $0s$-$0p$-$1s0d$-$1p0f$ model space is used. The Warburton-Brown interaction WBP10 was originally constructed by fitting energy levels in the 0–1$\hbar\omega$ space and has also been applied to study the energy spectra of $2p$-$2h$ states. In the WBP10 interaction, the coupling between the following multi-$\hbar\omega$ configurations is cut off: The two-body matrix elements for $1p$-$1h$ $2\hbar\omega$ excitations are all set equal to 0 due to the Hartree-Fock condition. The cross shell $2\hbar\omega$ two-body matrix elements between $0s^2$ and $0p^2$ have been also set equal to 0. The WBP10 interaction is enclosed in the NUSHELL@MSU package.

The standard Lawson method is used to remove center-of-mass spurious components in the wave function by adding a fictitious Hamiltonian, which acts only on the center-of-mass excitation [34,35].

The one-body transition density (OBTD) is the standard output of the shell-model code such as OXBASH and NUSHELL@MSU [33]. The OBTDs are unrelated to the radial wave function but related to the angular momentum part between the initial and final states. Thus the transition matrix element can be given by the transition operator and the transition density can be given by the density operator using the same OBTDs.

The reduced transition matrix element between the final state $|J_f\rangle$ and initial state $|J_i\rangle$ can be expressed by the OBTDs and reduced single-particle matrix elements of the valence orbitals,

$$\langle J_f||\hat{O}^\lambda||J_i\rangle = \sum_{k_\alpha k_\beta} \mathrm{OBTD}(fik_\alpha k_\beta\lambda)\langle k_\alpha||\hat{O}^\lambda||k_\beta\rangle, \quad (1)$$

where J_i and J_f include all the quantum numbers needed to distinguish the states, and OBTD is given by

$$\mathrm{OBTD}(fik_\alpha k_\beta\lambda) = \frac{\langle J_f||\left[a^+_{k_\alpha}\otimes\tilde{a}_{k_\beta}\right]^\lambda||J_i\rangle}{\sqrt{2\lambda+1}}. \quad (2)$$

The OBTD can also be defined to include the isospin freedom [36].

The radial transition densities are calculated with the same OBTDs [23],

$$\begin{aligned}\delta\rho_\lambda(r) =& \frac{\langle J_f|\left|\sum_i \frac{1}{r^2}\delta(r-r_i)Y_\lambda\right||J_i\rangle}{\sqrt{2J_i+1}}\\ =& \frac{1}{\sqrt{2J_i+1}}\sum_{k_\alpha,k_\beta}\mathrm{OBTD}(fik_\alpha k_\beta\lambda)\\ &\times\langle k_\alpha|\left|\frac{1}{r^2}\delta(r-r')Y_\lambda\right||k_\beta\rangle, \end{aligned} \quad (3)$$

where

$$\langle k_\alpha|\left|\frac{1}{r^2}\delta(r-r')Y_\lambda\right||k_\beta\rangle = \psi_{k_\alpha}(r)\psi_{k_\beta}(r)\langle k_\alpha||Y_\lambda||k_\beta\rangle, \quad (4)$$

and $\psi_{k_\alpha}(r)$ is the radial wave function of the valence orbital k_α.

In the calculations we use the $spsdpf$ model space including excitations up to 2–3$\hbar\omega$ for ^{14}N, ^{15}N, and ^{16}N. Other nuclei are studied in the $spsdpf$ model space including 1$\hbar\omega$ excitations.

III. THE PROPERTIES OF THE GROUND STATES IN THE NITROGEN CHAIN

The shell model with the WBP10 interaction has given the correct ground-state spins in $^{12-17}$N in the 0–1$\hbar\omega$ space. In ^{18}N, experimentally the first excited state 2^- is of 0.1149 MeV above the ground state and the shell model has missed the order of these two states. In ^{19,20}N the ground-state spins given by experiment are tentative. The values from the shell-model calculations are consistent with the experimental assumptions [37].

Figure 1 gives the proton and neutron separation energies of the ground states of the nitrogen chain. Charge independence and charge symmetry breaking are not included in the WBP10 effective interaction. To take into account the Coulomb effect on the proton separation energies, which is usually the main source of charge symmetry breaking, the normalized proton separation energies S_p are also given in Fig. 1; i.e., they have subtracted the difference of $S_p - S_n$ in ^{14}N. This difference, 2.943 MeV, is very close to the roughly estimated Coulomb barrier 2.987 MeV from the equation

$$U_{\mathrm{Coul.}} = \frac{kZ_1Z_2e^2}{R}, \quad (5)$$

where $Z_1 = 6$, $Z_2 = 1$, $ke^2 = 1.44$ MeV fm and $R = 1.2A^{1/3}$ fm. As can be seen from Fig. 1, the shell model with the WBP10 interaction has well reproduced the proton and neutron separation energies for the entire nitrogen chain, notably a drop in ^{16}N in which only one neutron sits outside of the $N = 8$ closed shell.

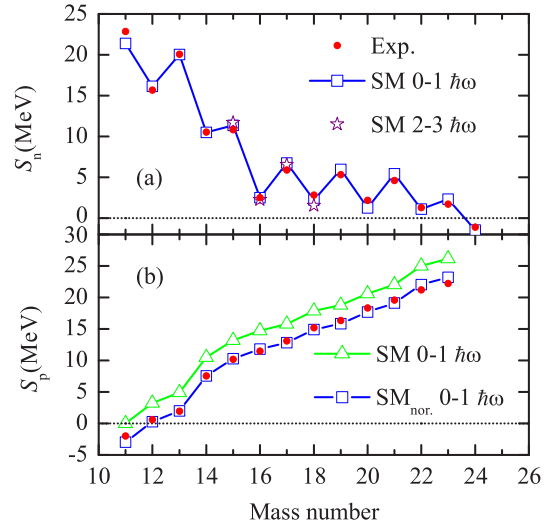

FIG. 1. Neutron and proton separation energies of the nitrogen isotopes. The solid circles are experimental values. The open squares and stars are the shell-model results in 0–1$\hbar\omega$ and 2–3$\hbar\omega$ spaces, respectively. In panel (b), the normalized proton separation energies which takes into account of the Coulomb barrier are also shown by open squares. The lines are only guides for the eyes.

In this paper, the self-consistent Skyrme-Hartree-Fock (SHF) wave functions with the KDE0 interaction [38] are used in the calculation of electric dipole matrix elements. The KDE0 effective interaction has survived a series of tests and is recommended as one of several Skyrme parametrizations for future studies [39]. The SHF equations are solved in the coordinate space. The wave functions of the unoccupied states are obtained by solving the nuclear mean-field potential within a sphere of 15 fm in radius. And for each unbound orbital, the nuclear potential is stretched so that its energy is below the potential barrier and the root-mean-squares radius of this orbital is inside the barrier. To check the single-particle wave functions, the mass radii of the nitrogen isotopes are calculated and compared with the experimental data in Fig. 2. The results with the SHF approach are also presented. It is seen that the mass radii calculated by the shell model and the SHF approach are very close. The shell-model results for $^{17-23}$N are slightly larger than those from the SHF approach, largely due to the mixing of the orbitals which have long tails. Generally, two models have reproduced the trend of the experimental data. It seems the theoretical results are more in line with the experimental data given by Liatard *et al.* [41] for ^{16,17,18,19}N, while these values in Ref. [40] are somewhat smaller. However, the experimental results deduced from total reaction cross sections exhibit significant negative isospin shifts at the shells, i.e., $N = 6$, 8, and 14 [40]. This feature is not reproduced by either model.

IV. ELECTRIC DIPOLE STRENGTHS AND PYGMY DIPOLE RESONANCES IN NITROGEN ISOTOPES

The electric dipole transition strength $B(E1)$ is defined as

$$B(E1;\omega_n) = \sum_{\mu} \left|\langle n|\hat{O}^{\lambda+1}_{\mu}|\text{g.s.}\rangle\right|^2, \qquad (6)$$

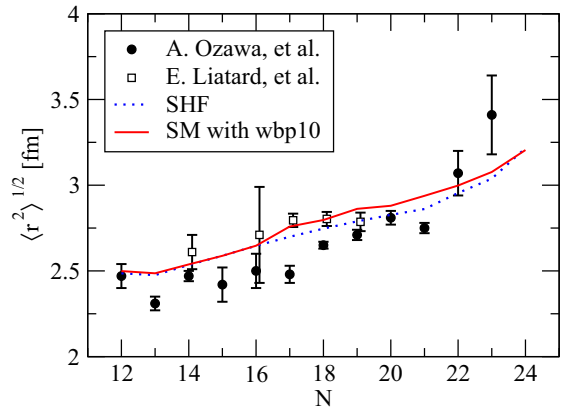

FIG. 2. Mass radii of the nitrogen isotopes. The solid cycles indicate the experimental data compiled by Ozawa *et al.*; see Ref. [40] and references in. The open squares indicate the experimental results given in Ref. [41]. The solid line gives the shell-model results in 0–1$\hbar\omega$ space using the SHF single-particle wave functions.

where the matrix element is calculated between the ground state ($|$g.s.$\rangle$) and the nth$E1$ excited shell-model state ($|n\rangle$) with the excitation energy $\hbar\omega_n$. For $E1$ transitions, the parities of initial and final states should be opposite in order to conserve the total parity. Because in Eq. (7) there are only isoscalar and isovector excitations, and the isospin of the nuclear ground state is normally its minimum value, i.e., $T = (N - Z)/2$, the electric-dipole absorption of photons by a nucleus can only lead to the states with isospin $T = T_z$ or $T = T_z + 1$ with the first possibility disappearing when $T_z = 0$.

To further remove the additional spurious components due to the usage of the Skyrme-Hartree-Fock wave functions, the center-of-mass removed dipole operator [42] is used in the calculation of the dipole transition strength,

$$\tilde{Q}^{\lambda=1}_{\mu} = e\frac{N}{A}\sum_{i}^{Z} r_i Y_{1\mu}(\hat{r}_i) - e\frac{Z}{A}\sum_{i}^{N} r_i Y_{1\mu}(\hat{r}_i), \qquad (7)$$

where Z, N, and A are proton, neutron, and mass numbers, respectively. The effectiveness of this method was demonstrated in Refs. [30,31]. To smooth out the discrete strengths, the transition strengths are averaged by a Lorentz-type factor $\rho(\omega)$,

$$\frac{d\bar{B}(E1;\omega)}{d\omega} = \int \sum_{n} B(E1;\omega_n)R(\omega-\omega_n)d\omega, \qquad (8)$$

where ω is the photon energy and

$$R(\omega-\omega_n) = \frac{1}{\pi}\frac{\Gamma/2}{(\omega-\omega_n)^2+\Gamma^2/4}. \qquad (9)$$

In this paper, an arbitrary total width $\Gamma = 2$ MeV is used. In principle, the R-matrix theory can be used to calculate the partial and total width of resonances. However, the total absorption will remain practically unchanged because the calculated total width values are not much different from the fixed $\Gamma = 2$ MeV [43]. In this way, the response function is like the superposition of many isolated Breit-Wigner resonances.

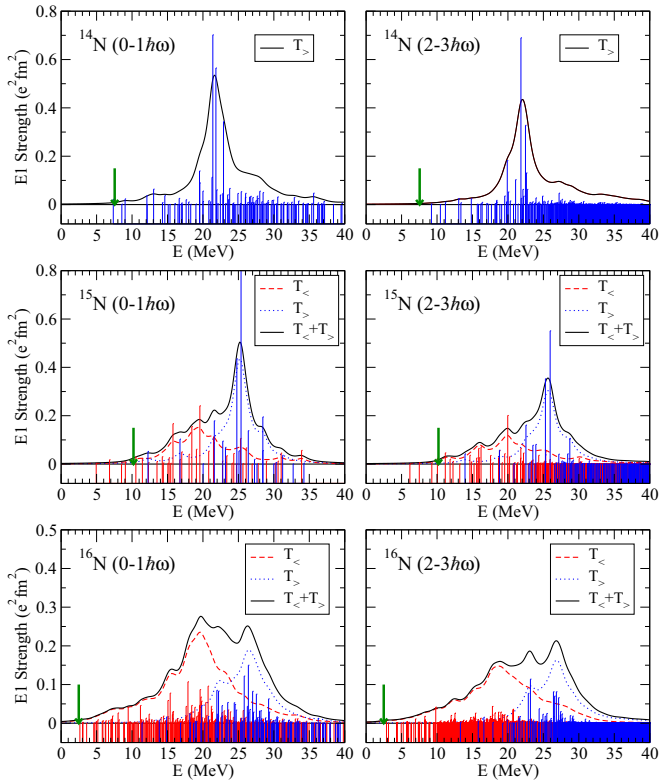

FIG. 3. The calculated electric dipole strengths from the excited to the ground states for ^{14,15,16}N in the shell-model space up to 0–1$\hbar\omega$ and 2–3$\hbar\omega$ excitations. The thin drop lines are the discrete $B(E1)$ values in the shell-model calculations. The dashed (red), dotted (blue), and solid (black) lines represent the transitions from $T = T_z$, $T = T_z + 1$ states (labeled as $T_<$ and $T_>$) and their sums, respectively. The arrows separate the continuum from the discrete states.

The electric dipole strengths from the excited to the ground states for ^{14,15,16}N are shown in Fig. 3. The states of $T = T_z$ and $T = T_z + 1$ are denoted as $T_<$ and $T_>$. The general features by including 2–3$\hbar\omega$ excitations have been discussed in the study of oxygen and carbon isotopes [30,31]. It is indeed clearly seen that the peak strengths are reduced in the 2–3$\hbar\omega$ calculations, although the discrete level density generally increases. The remaining strength is pushed up beyond $E > 40$ MeV, similar to the discussions in the carbon isotopes [31]. Recent large-scale shell-model calculations in calcium isotopes by Y. Utsuno *et al.* [44] also suggest the inclusion of 3$\hbar\omega$. Figure 4 gives the electric dipole strengths for $^{17-20}$N in the 0–1$\hbar\omega$ space. Compared with the results of ^{14,15,16}N in the same space, we can see that except for ^{15}N, which has a neutron closed shell, the discrete level density generally increases with increasing isospin, and meanwhile discrete $B(E1)$ strengths becomes more spread out.

In ^{14}N, only the de-excitation of $T_>$ states contributes to the dipole strength. The GDR is largely a single-peak shape. As isospin increases, the competition between the $T_<$ and the $T_>$ states gives the GDR more complex structure. If the GDR peaks of $T_<$ and $T_>$ have similar height, i.e., in ^{16,17}N, a plateau is seen. As the isospin further increases, the $T_<$ one will dominate and then the GDR is largely a single peak again.

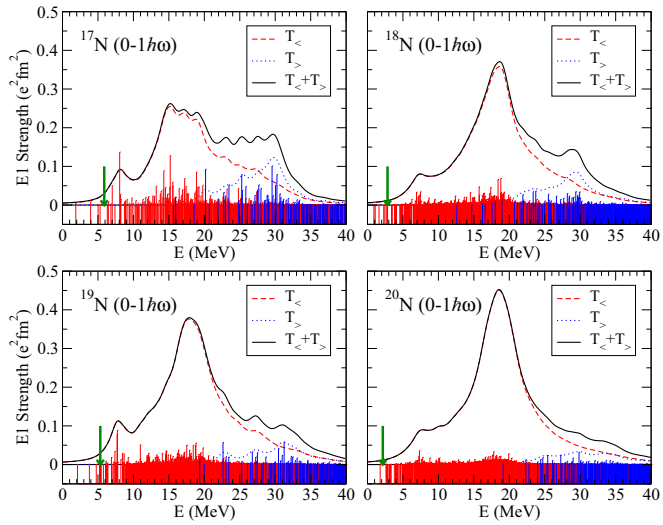

FIG. 4. Same as Fig. 3 but for $^{17-20}$N in the *spsdpf* space up to 0–1$\hbar\omega$ excitations.

For the further discussion on the splitting of isospin doublets, see Sec. V.

As can be seen from Fig. 3, in the low-energy region ($E <$ 10 MeV), very little dipole strength is seen in ^{14,15}N, while some amount appears in ^{16}N. As the nucleus is located further away from the β-stability line, it is seen in Fig. 4 that the low-lying dipole strength greatly increases in $^{17-20}$N. The picture remains largely the same if we use the harmonic oscillator wave function instead of the ones calculated by the SHF approach, although the pygmy strengths are lowered about ∼10%. It would be very interesting to investigate the nature of the enhanced pygmy strengths in $^{17-20}$N. To this end, the transition densities of those discrete levels which have prominent $B(E1)$ values in the PDR and GDR regions are drawn and shown in Figs. 5, 6, 7, and 8 for ^{17,18,19,20}N, respectively. The common feature is that the transition densities near the GDR peaks have the opposite phase, i.e., the bulk protons and neutrons move against each other. In ^{19}N, the transition densities at $E = 10.978$ MeV with $J^\pi_f = 5/2^+$ and $T = T_z$ are also of GDR type. However, for those states which contribute to the low-energy bump in Fig. 4, with the energies $E \lesssim 8$ MeV, the protons and neutrons move in phase in the nuclear interior, while they are gradually out of phase roughly beyond the mass radii. This scenario is similar to the observation of the mean-field plus RPA theory in neutron-rich oxygen isotopes that this is the typical pygmy resonances of the halo-skin neutrons oscillating against the inner core [21,45]. For these neutron-rich nuclei, the neutron wave functions of the weakly bound orbitals extend far away from the core; therefore long tails appear in the neutron transition densities of the PDR states. In contrast, the transition densities of GDR states show little tail beyond the $2\sqrt{\langle r^2\rangle} \sim 6$ fm.

In light nuclei the GDR is not completely collectivized [43]. The giant peak in ^{14}N is dominated by the $2s1d \leftrightarrow 1p$, particularly $1d_{5/2} \leftrightarrow 1p_{3/2}$, transitions. In ^{15,16}N, the GDRs are also largely $2s1d \leftrightarrow 1p$ transitions, only more diversified. From ^{17}N to ^{20}N, as the neutron Fermi level

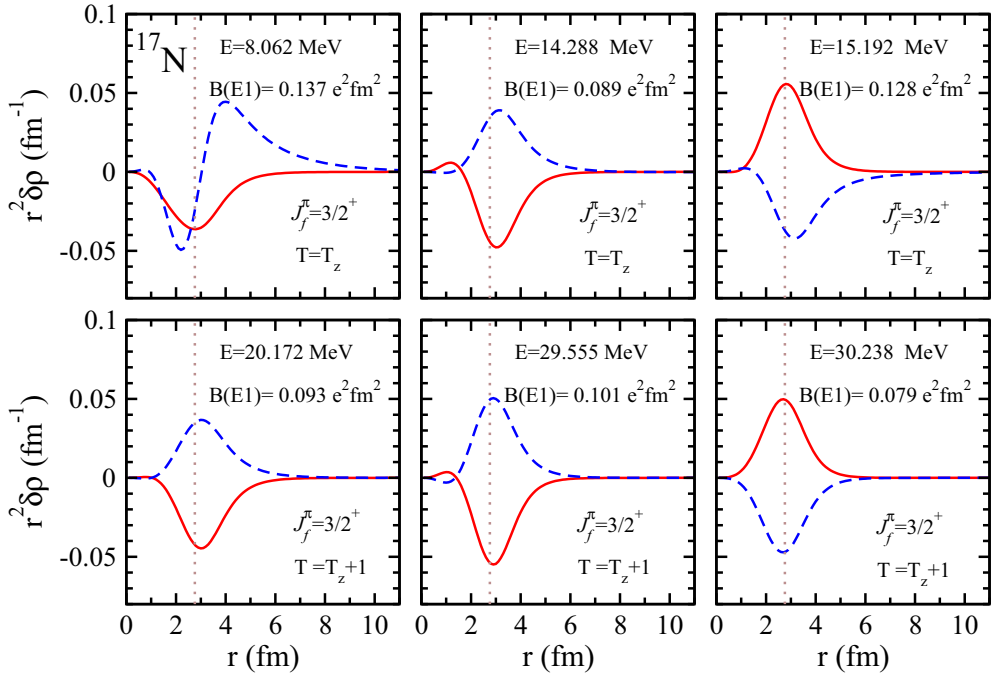

FIG. 5. Shell-model transition densities of discrete dipole transitions in ^{17}N. The solid red and dashed blue lines are for proton and neutron, respectively. The dotted brown line gives the location of the mass radius in the shell-model calculations.

is approaching the $N = 20$ shell gap, although the GDRs are still largely the $2s1d \leftrightarrow 1p$ transitions, some amount of contribution comes from the $1f2p \leftrightarrow 2s1d$ transitions for the $T = T_z$ states. Meanwhile, because the proton number is less than 8 while the neutron number is larger than 8, only the $2s1d \leftrightarrow 1p$ transitions contribute to the GDRs for the $T = T_z + 1$ states. However, for the PDRs in $^{17-20}$N, the $1f2p \leftrightarrow 2s1d$ transitions seemingly play a larger role except for the $E = 7.743$ MeV state in ^{19}N. Even in that case the $1f2p \leftrightarrow 2s1d$ transitions still contribute considerably. The matrix elements of transitions between the valence orbitals for the selected PDR states are shown Fig. 9. It is also seen that the PDRs are usually not dominated by one transition, which is distinctive from the GDRs in the light nuclei. If this is some collectivity suggested by authors in Ref. [23], then together with the discussions on the transition densities, the PDRs in

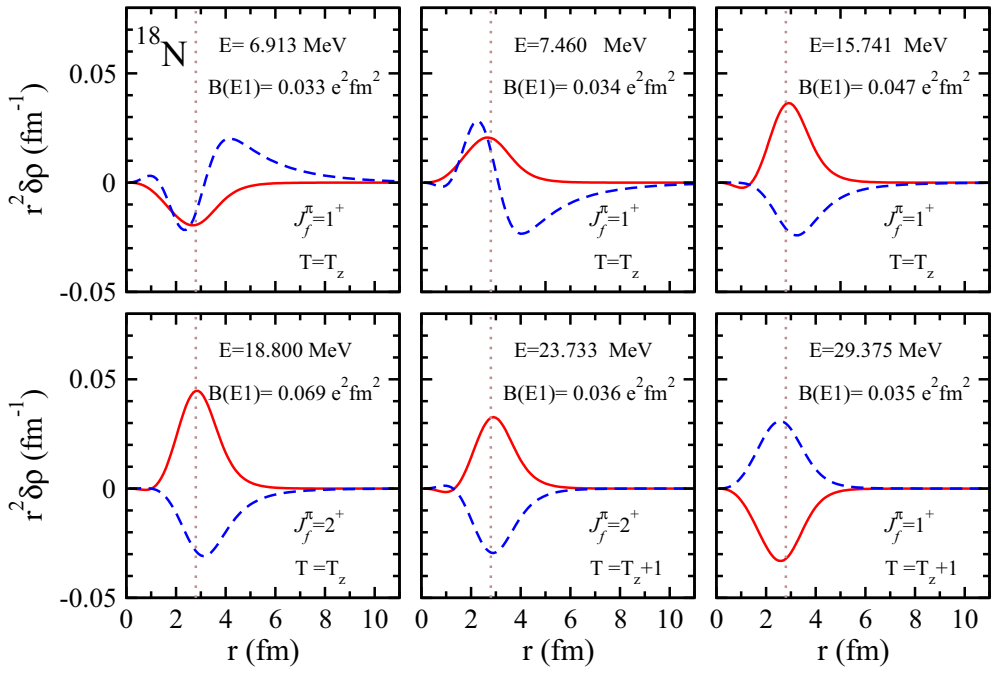

FIG. 6. Shell-model transition densities of discrete dipole transitions in ^{18}N.

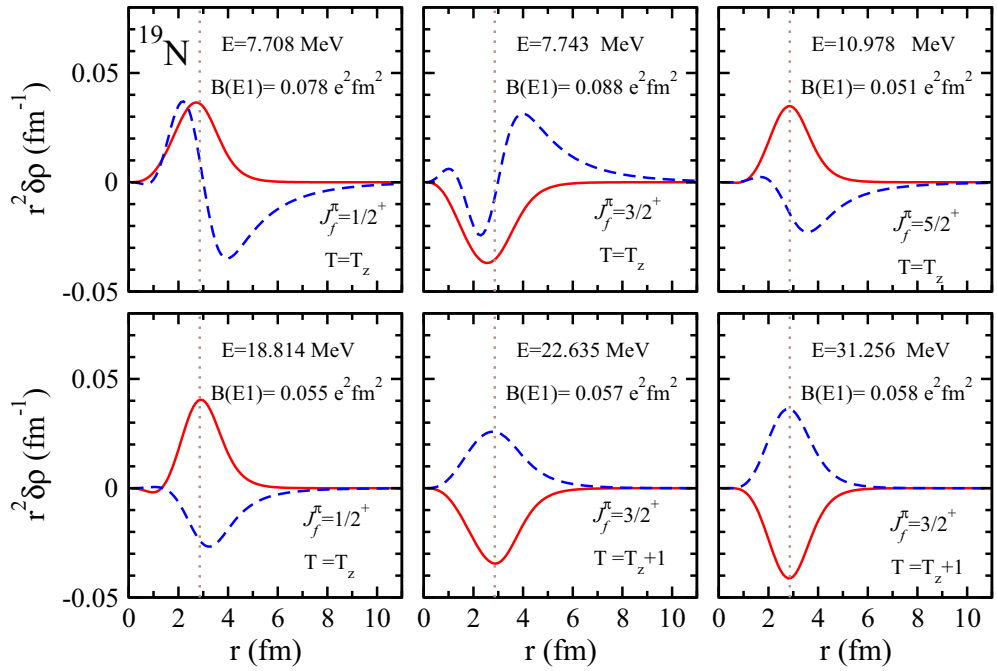

FIG. 7. Shell-model transition densities of discrete dipole transitions in ^{19}N.

$^{17-20}$N are collective due to the soft mode between the excess neutrons and the core.

V. SUM RULE AND SYSTEMATICS OF ISOSPIN DOUBLETS IN NITROGEN ISOTOPES

The sum rules are useful measures of the collectivity of the giant resonances. In Table I, the ground-state spins, the GDR peaks, the nonenergy-weighted sum rule (NESR), and the energy-weighted sum rule (EWSR) of dipole strengths in the nitrogen isotopes are shown. The total sum rule is obtained by summing up to 40 MeV. For the isovector GDR, the classical energy-weighted sum rule value is given by

$$S(\mathrm{TRK}) = \sum_n \hbar\omega_n \left|\langle n|\hat{O}_\mu^{\lambda=1}|\mathrm{g.s.}\rangle\right|^2 = \frac{\hbar^2}{2m}\frac{9}{4\pi}\frac{NZ}{A}$$
$$= 14.9\frac{NZ}{A}e^2 \ (\mathrm{MeV\,fm^2}), \qquad (10)$$

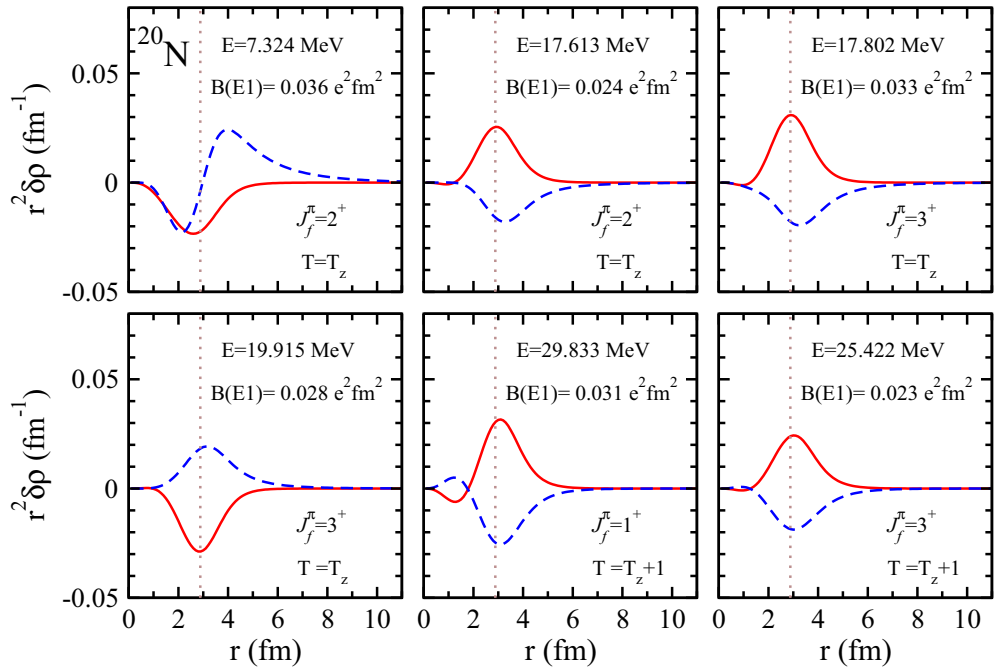

FIG. 8. Shell-model transition densities of discrete dipole transitions in ^{20}N.

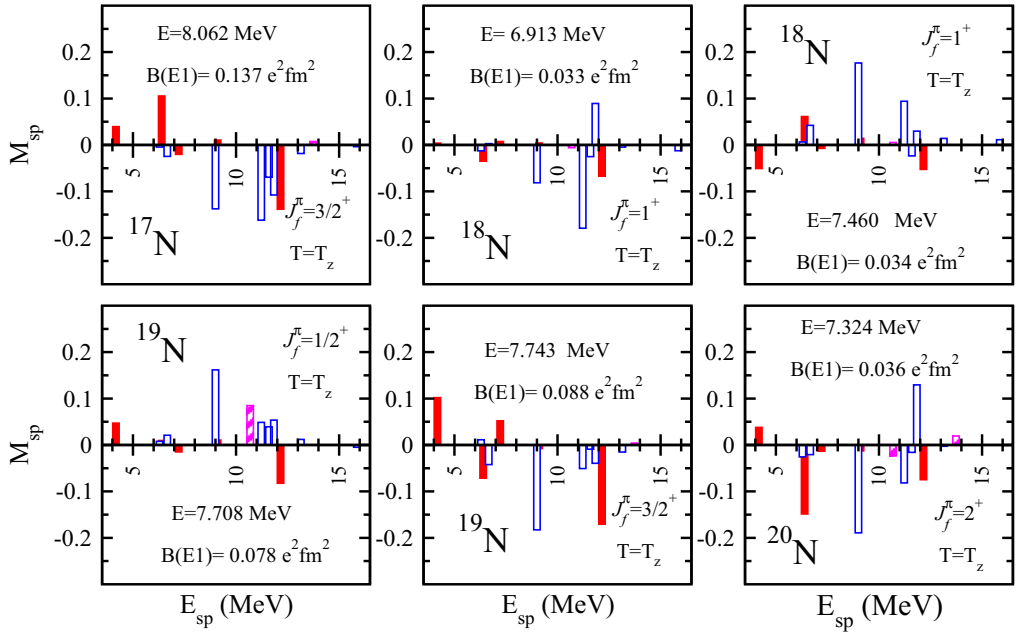

FIG. 9. Contributions to the total matrix elements of valence orbitals for the de-excitations from the selected PDR states in $^{17-20}$N. The horizontal axis is the single-particle excitation energies of valence orbitals. The magenta bars with slanted lines, the solid red bars, and the open blue bars indicate the transitions between the valence orbitals of $1s \leftrightarrow 1p$, $1p \leftrightarrow 2s1d$, and $2s1d \leftrightarrow 1f2p$, respectively.

neglecting the contributions of exchange terms. This sum rule is known as the Thomas-Reiche-Kuhn (TRK) sum rule.

It is seen from Table I that the GDR centroids of ^{14,15,16}N are pushed up ∼0.5 MeV with the inclusion of 2–3$\hbar\omega$ excitations. For the 0–1$\hbar\omega$ calculations, the GDR energies and the sum rules show some isospin dependency. To show this feature more clearly, the GDR energies and the splittings of the isospin doublets are drawn in Fig. 10. It is seen that the GDR energies for the $T_>$ states generally increase with increasing isospin, although the increasing shows some staggering with the neutron number. However, for the $T_<$ states, the variation of GDR energies with the isospin is more intricate, i.e., lacking clear isospin dependency. In contrast, the GDR energy for the heavy nuclei, where the transition of $T_<$ states dominates, is proportional to the linear combination of $A^{-1/6}$ and $A^{-1/3}$ [3,46]. In Fig. 10(b), the GDR energy differences between $T_<$ and $T_>$ states calculated by the shell model are compared with the systematics of energy displacement of dipole isospin doublets derived from the symmetry energy, i.e., Ref. [47],

$$E_> - E_< = \frac{60(T+1)}{A}\text{MeV}. \tag{11}$$

We can see that the trend of the shell-model results is consistent with the systematic splittings, especially near the β-stability line. The staggering on even-odd neutron number is also more apparent. However, when the nucleus is far away from the β-stability line, the systematic deviation from the values with Eq. (11) can be significant.

As discussed in the last section, the dipole responses are less enhanced in the 2–3$\hbar\omega$ space calculations than those in the 0–1$\hbar\omega$ space calculations. Correspondingly the NESR and EWSR values in the 2–3$\hbar\omega$ space calculations, as well as the EWSR values against the TRK sum rule, are also less enhanced, about 80% of those values in the 0–1$\hbar\omega$ calculations for ^{14,15,16}N. In the normal shell-model calculations, the excitation of nucleons is restricted in several adjacent major shells, and thus a large number of configurations, although usually at higher energies, are neglected. The decorrelation of those configurations pushes the strengths to lower energies and hence enhances response functions.

In the 0–1$\hbar\omega$ space calculations, the EWSR values for the $T_>$ states are decreasing with increasing isospin, while it is vice versa for the $T_<$ states. However, the ratio of EWSR in the shell-model calculations over the TRK values remain largely stable around 1.4–1.5. In medium and heavy nuclei, the systematic ratio of EWSR values between the $T_<$ and $T_>$ states reads [48]

$$\frac{\text{EWSR}(T_>)}{\text{EWSR}(T_<)} = \frac{\sigma_>}{\sigma_<} = \frac{1}{T}\frac{1-\frac{3}{2}TA^{-2/3}}{1+\frac{3}{2}TA^{-2/3}}. \tag{12}$$

The shell-model EWSR ratios are compared with the systematic values in Fig. 11. We can see that generally the shell model has reproduced the trend of the systematic values throughout the entire nitrogen chain. However, the consistent overestimation of the EWSR ratios indicates that the enhancement of response functions are incoherent for the $T_<$ and $T_>$ states. In other words, the enhancement for the $T_>$ states are relatively larger than that for the $T_<$ states. Considering that only those states below 40 MeV have been included in the calculation of EWSR values, some amount of sum rule would be missing for the $T_>$ states (the EWSR values would be about 3%, 5% 9%, and 13% larger for ^{17,18,19,20}N if we sum up to 50 MeV), then the overestimation of the ratio would be even larger. It is also interesting to notice that the calculated EWSR

TABLE I. Ground-state spins, nonenergy-weighted sum rule, and energy-weighted sum rule of $E1$ transitions in the nitrogen isotopes. The peak energies in the response function and the photoadsorption cross sections are usually very close, but if there are competing peaks, e.g., the $T_<$ states in ^{17}N and the $T_>$ states in ^{20}N, the chosen GDR peaks are set between the peaks. The total sum rule values are obtained by summing up to $E_x = 40$ MeV, while for the sum rule of the PDRs, the sums are extend to $E_x = 10$ and 15 MeV in the last two columns respectively. In ^{19,20}N, the ground-state spins and parities are only tentatively set according to the shell-model calculation; also see the discussion in Ref. [37].

Nuclides	$J^\pi_{\text{g.s.}}$	Isospin	E_{peak} (MeV)	NESR (e^2fm^2)	EWSR (MeVe^2fm^2)	S(TRK) (MeVe^2fm^2)	EWSR/TRK (%)	EWSR $<$ 10 MeV) (MeVe^2fm^2) (%)	EWSR ($<$15 MeV) (MeVe^2fm^2) (%)
^{14}N($1\hbar\omega$)	1^+	$T = 1$	21.6	3.283	74.17	52.15	142.2	0.67(1.3)	3.32(6.4)
$[(1+3)\hbar\omega]$		$T = 1$	22.0	2.591	60.98	52.15	116.9	0.24(0.5)	1.51(2.9)
^{15}N($1\hbar\omega$)	$1/2^-$	$T_< = 1/2$	19.4	1.508	30.63			0.49	2.57
		$T_> = 3/2$	25.2	2.206	53.97			0.17	1.12
		Total		3.714	84.60	55.63	152.1	0.65(1.2)	3.69(6.6)
$[(1+3)\hbar\omega]$	$1/2^-$	$T_< = 1/2$	19.9	1.244	25.65			0.33	2.41
		$T_> = 3/2$	25.7	1.654	41.59			0.10	0.73
		Total		2.898	67.24	55.63	120.9	0.43(0.8)	3.14(5.6)
^{16}N($1\hbar\omega$)	2^-	$T_< = 1$	19.6	2.339	48.85			1.46	5.79
		$T_> = 2$	26.5	1.504	38.49			0.09	0.51
		Total		3.843	87.34	58.67	148.9	1.55(2.6)	6.30(10.7)
$[(1+3)\hbar\omega]$	2^-	$T_< = 1$	19.0	1.799	34.41			1.01	4.58
		$T_> = 2$	26.9	1.162	30.92			0.06	0.27
		Total		2.961	65.33	58.67	111.3	1.07(1.8)	4.85(8.3)
^{17}N($1\hbar\omega$)	$1/2^-$	$T_< = 3/2$	17.8	2.940	63.18			2.58	11.68
		$T_> = 5/2$	29.8	1.107	29.21			0.05	0.25
		Total		4.047	92.38	61.35	150.6	2.63(4.3)	11.93(19.4)
^{18}N($1\hbar\omega$)	1^-	$T_< = 2$	18.7	3.504	71.73			2.79	10.94
		$T_> = 3$	29.4	0.806	21.51			0.04	0.15
		Total		4.502	93.24	63.74	146.3	2.82(4.4)	11.09(17.4)
^{19}N($1\hbar\omega$)	$(1/2^-)$	$T_< = 5/2$	18.4	3.923	80.12			3.24	12.58
		$T_> = 7/2$	31.2	0.559	16.49			0.02	0.08
		Total		4.483	96.61	65.87	146.7	3.26(4.9)	12.66(19.2)
^{20}N($1\hbar\omega$)	(2^-)	$T_< = 3$	18.6	4.120	85.25			3.22	11.99
		$T_> = 4$	31.0	0.397	12.08			0.01	0.05
		Total		4.517	97.33	67.80	143.6	3.24(4.8)	12.04(17.8)

ratio over the systematic ratio is increasing with the increasing isospin almost linearly. The linearity would be even better if the sums are up to 50 MeV. There is no immediate explanation for this linearity; thus it poses an interesting question for theorists working on the shell model.

VI. SYSTEMATIC COMPARISON OF PDRS IN NITROGEN, CARBON, AND OXYGEN ISOTOPES

In Sec. IV, it is shown that sizable pygmy dipole resonances appear in the low-energy region in ^{17,18,19,20}N. In the last two columns of Table I, the EWSR values summing up to 10 MeV and their ratios to the classical TRK sum rule are given for the nitrogen isotopes. It is seen the EWSR of the PDRs exhausts nearly 5% of the classical sum rule. If we sum up to 12 MeV, the EWSR would exhaust 7.2%, 7.6%, 8.6%, and 8.2% for ^{17,18,19,20}N and if we sum up to 15 MeV they will further increase to exhaust 19.4%, 17.4%, 19.2%, and 17.8% of the classical sum rule, respectively.

The evolution of PDRs in an isotopic chain has been discussed in several isotopes, such as C [31], O [19,21,30], Ca [10,49–51], Ni, Sn [16,21], and Pb [52]. It is also interesting to compare the PDRs of neighboring nuclei, since not only the neutron-proton disparity $N - Z$ but also the mass A weights in EWSRs. In this paper, the dipole resonances of neighboring nuclei of nitrogen, i.e., the carbon and oxygen isotopes (including ^{19,21,23}O, whose results were not provided in Ref. [30]), were recalculated using the KDE0 Skyrme parameters and the EWSR values are summed up to 10 and 15 MeV. The exhaustion of EWSR values in these isotopes is then compared in Fig. 12. For each isotopic chain, marked increases of EWSR in the low-energy region are first seen when the neutron-proton disparity $N - Z$ increases from zero. However, at some point ($N - Z \sim 2$–3 for summing up to 10 MeV, $N - Z \sim 3$–4 for summing up to 15 MeV), the exhaustion of EWSR values then seems to stop increasing steeply and even drops in some cases. Only for the sum up to 10 MeV does the EWSR pick up at very large $N - Z$. In neutron-rich oxygen isotopes, the experimental dipole strength

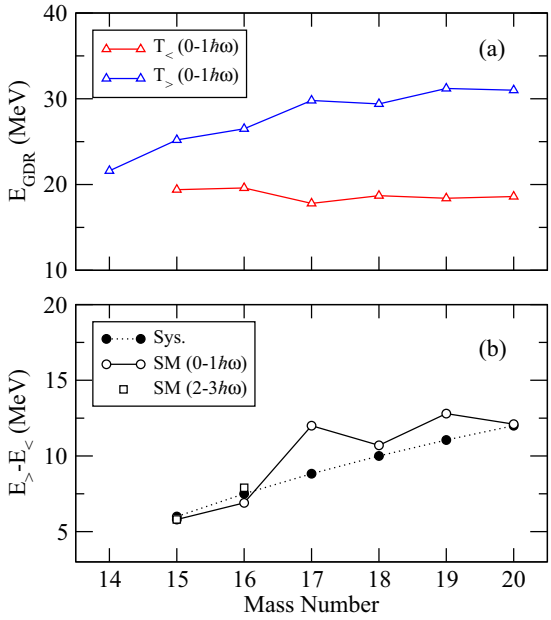

FIG. 10. (a) GDR energies and (b) splitting of isospin doublets in the nitrogen isotopes. The stars indicate the systematic values obtained from Eq. (11). The open circles and solid squares represent the shell-model results in the 0–1$\hbar\omega$ and 2–3$\hbar\omega$ spaces.

summed up to 15 MeV exhausts up to 12% of the classical sum rule [22], of which the trend is in good agreement with the shell-model results albeit general overshooting in the 0–1$\hbar\omega$ space. In Fig. 12(a) some twists can be seen at close shell nuclei ^{14}C and ^{20}C and ^{22}O, mostly due to relative low-level density in the low-energy region. These twists are not obvious or even disappear in Fig. 12(b).

It is also interesting to note that the low-lying strengths of $^{15-18}$C are almost twice those in oxygen with the same $N-Z$. For the nitrogen isotopes the EWSR values summing up to 10 MeV are close to the carbon isotopes for $N-Z \geqslant 3$. However, by summing up to 15 MeV, the EWSR values show a clear tendency of decreasing with the increasing Z with the same

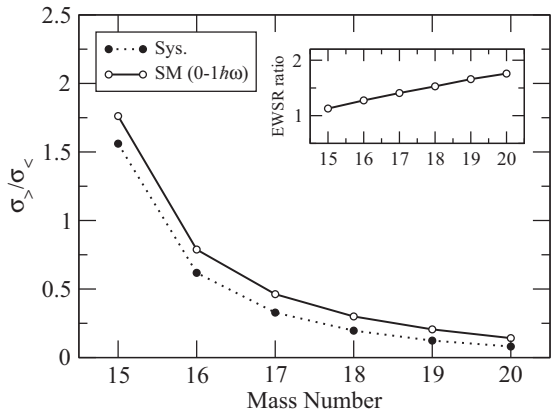

FIG. 11. Ratios of $T_<$ and $T_>$ EWSR values in the nitrogen isotopes. The subfigure shows the shell-model ratios over the systematic values.

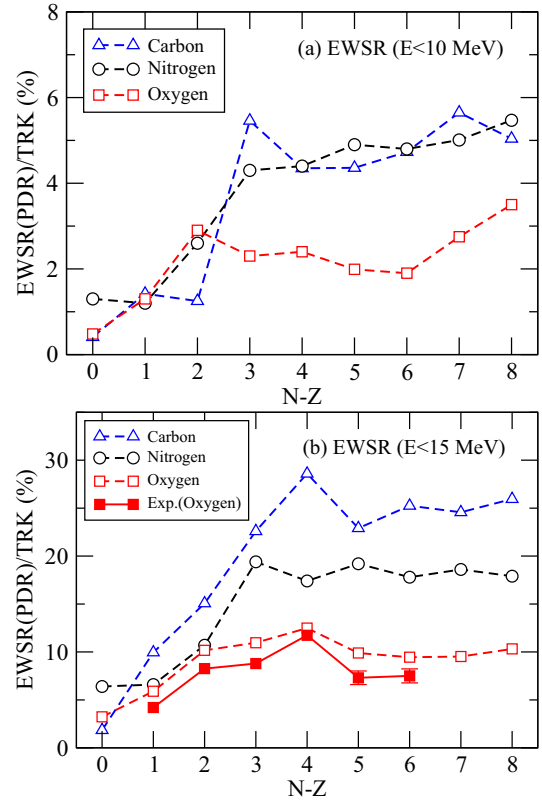

FIG. 12. The EWSR values of the PDRs in nitrogen, carbon, and oxygen isotopes. The EWSR values are summed up to (a) 10 and (b) 15 MeV. The experimental values of oxygen isotopes are taken from Ref. [22].

$N-Z$. There is another sum rule, named the energy-weighted cluster sum rule, which can be viewed as a measure of the adiabaticity between the giant and pygmy resonances [53]. Assuming that the nucleus (A,Z) can be decomposed into two clusters with (A_1,Z_1) and (A_2,Z_2), the cluster sum rule is given by

$$S(\text{cluster}) = \frac{\hbar^2}{2m}\frac{9}{4\pi}\frac{(Z_1A_2 - Z_2A_1)^2}{AA_1A_2}. \tag{13}$$

If we take $(A_1 = 2Z, Z_1 = Z)$ as the core and $(A_2 = A - 2Z, Z_2 = 0)$ as the valence nucleons, then the ratio of cluster over TRK sum rules is given by

$$\frac{S(\text{cluster})}{S(\text{TRK})} = \frac{N-Z}{2N}. \tag{14}$$

Thus for nuclei with the same $N-Z$, the $S(\text{cluster})/S(\text{TRK})$ ratio will decrease with increasing N or equivalently with increasing Z. The consistency between the EWSR values and the cluster sum rules supports the idea that the PDRs in the neutron-rich light mass nuclei, especially those with the closed proton shell, are caused by the soft mode where the excess neutrons oscillate against the isospin saturated core.

VII. PHOTOABSORPTION CROSS SECTIONS IN NITROGEN ISOTOPES

As far as only the dipole strength is concerned, the photoabsorption cross section can be expressed as follows:

$$\sigma(\omega) = \frac{16\pi^3}{9\hbar c}\omega\frac{d\bar{B}(E1;\omega)}{d\omega}. \quad (15)$$

As discussed in Sec. V, the dipole responses calculated in the restricted shell-model space result in an enhancement of EWSR compared with the classical TRK sum rule. In order to obtain a quantitative agreement with available experimental cross sections of ^{14,15}N, the theoretical cross sections need to be renormalized. We introduce two renormalization factors for the $T_<$ and $T_>$ states respectively, i.e.,

$$\sigma(\omega) = \eta_<\sigma_<(\omega) + \eta_>\sigma_>(\omega). \quad (16)$$

In the 2–3$\hbar\omega$ space calculation of ^{15}N, it is found the theoretical cross sections are very close to the experimental data for $E \lesssim 20$ MeV; see Fig. 13(d). It indicates that $\eta_< \approx 1$ in this case and the enhancement of EWSR mainly results from

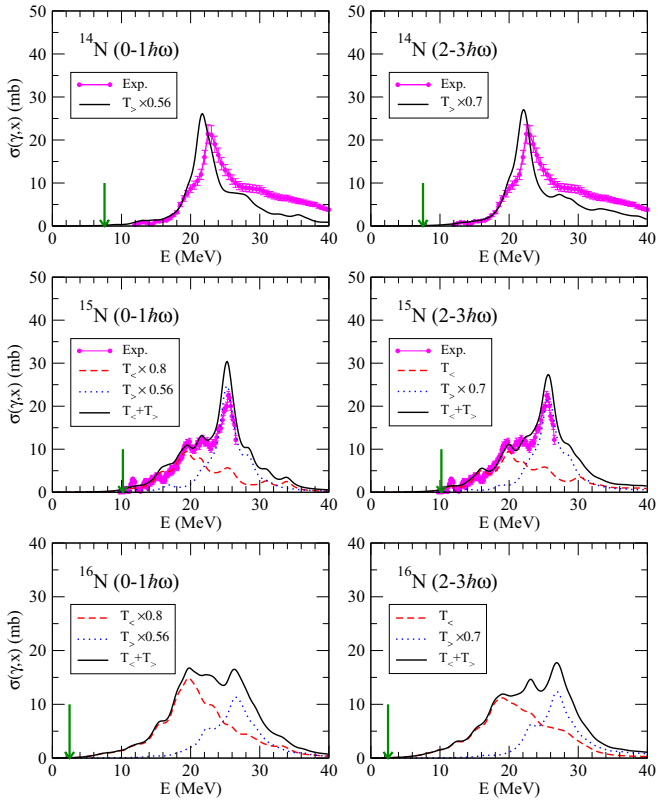

FIG. 13. Theoretical and experimental photo absorption cross sections in ^{14,15,16}N. The solid lines with error bars are experimental data. The solid without error bars are total photoabsorption cross sections in the shell-model calculations, and dashed and dotted lines are contributions from $T_<$ and $T_>$ states. The experimental data of ^{14}N are taken from the evaluated version [54], and we add 10% of the data as the error bars. The experimental data of ^{15}N are taken from Ref. [55]. For the reduction factors in the legends, see the text for details.

TABLE II. The reduction factors in the shell-model calculation of the photoabsorption cross sections.

	$\eta_<$	$\eta_>$
0–1$\hbar\omega$	0.8	0.56
2–3$\hbar\omega$	1.0	0.70

$T_>$ states. In Ref. [31], the authors analyzed the enhancement of EWSR in ^{12}C where only $T_>$ states contribute to the photoabsorption cross sections. They estimated that 25 ± 10% of the calculated strength obtained within the 2–3$\hbar\omega$ space should be in the energy region higher than 35 MeV, thus the calculated cross sections for ^{12}C were multiplied by a factor 0.7. The cross sections for ^{14}N also are reasonably reproduced with this reduction factor in the 2–3$\hbar\omega$ calculations; see Fig. 3(b). In the 0–1$\hbar\omega$ calculations, considering that the EWSR values are about 25% larger than the values in the 2–3$\hbar\omega$ space calculations, the $\eta_<$ value would be further reduced to $0.7/1.25 = 0.56$. A summary of reduction factors is given in Table II.

With the reduction factors discussed above, the theoretical photoabsorption cross sections in the ^{14,15,16}N isotopes are compared with available experimental data in Fig. 13. After the normalization, both the 0–1$\hbar\omega$ and 2–3$\hbar\omega$ space calculations have reasonably well reproduced the experimental data in ^{14,15}N. For ^{14}N, there is only one giant peak, which is located at 22.2 MeV in the 2–3$\hbar\omega$ calculations, very close to the experimental one at 22.5 MeV. Both theoretical and experimental data show a high-energy tail (>25 MeV). In ^{15}N, besides the giant peak, there are several fragmented bumps around 15.5 and 20 MeV, which are due to transition of $T_<$ states. This feature is also clearly seen in the experimental data. In ^{16}N, the GDR peaks of $T_<$ and $T_>$ states are of similar

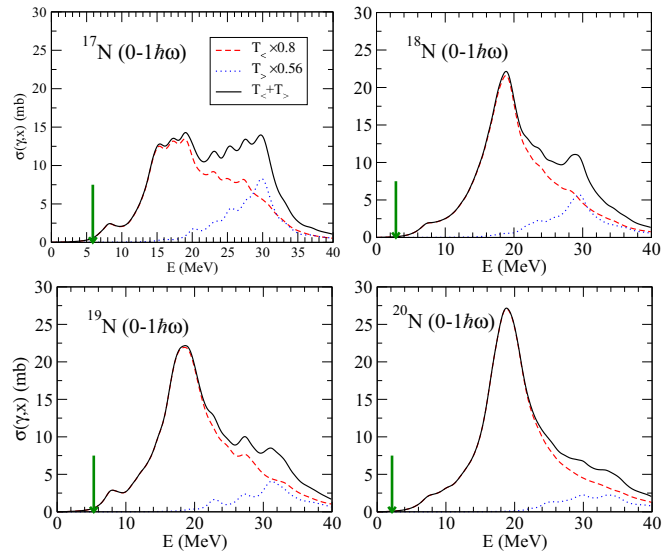

FIG. 14. Same as Fig. 13, but for ^{17,18,19,20}N in the 0–1$\hbar\omega$ space calculations. The same set of reduction factors is used in all subfigures; see the text for details.

height. Correspondingly, the cross sections are more spread up than those in ^{14,15}N. This feature will also be seen in ^{17}N.

Figure 14 gives the normalized photoabsorption cross sections for ^{17,18,19,20}N in the 0–1$\hbar\omega$ space calculations. Because different reduction factors are used for the $T_<$ and $T_>$ states, the GDRs are more increasingly dominated by the single $T_<$ peaks as the isospin increases. The overall peak height also increases with the increasing isospin, which is consistent with increasing TRK sum rule. The center of the PDR locates at $\sim$ 7 MeV, a few MeVs to the neutron separation threshold for the even neutron ^{17,19}N. Therefore, the astrophysical neutron capture cross sections for ^{16,18}N can increase tremendously.

VIII. SUMMARY

In summary, we have used the shell model to study the pygmy and giant dipole resonances in the nitrogen isotopes. The shell-model OBTDs and SHF single-particle wave functions were combined to to calculate matrix elements of electric dipole transitions. We checked the effective interaction and single-particle wave functions by comparing the nucleon separation energies and nuclear mass radii with available experimental data. The proton and neutron separation energies for the entire nitrogen chain are well reproduced by the WBP10 interaction. The SHF mean field was solved in the coordinate space to obtain the single-particle wave functions. The general trend of the experimental mass radii has been reproduced by combining shell model with the SHF single-particle wave functions, although the theory failed to reproduce the large negative isospin shifts at the shells of $N = 6$, 8, and 14.

Large enhancement of low-lying dipole strength, i.e., pygmy dipole resonances, was predicted in the neutron-rich ^{17,18,19,20}N. The nature of these PDRs was analyzed via the transition densities and transition matrix elements. It turns out these PDRs involve a larger amount of excitations between the $2s1d$ and loosely bound $1f2p$ shells. Combined with the transition densities, we concluded that the PDRs in ^{17,18,19,20}N are collective and due to the oscillation between the excess neutrons and the isospin saturated core, contrary to those states in the neutron-rich oxygen isotopes studied by the mean-field plus RPA approaches.

We also investigated the isospin dependence of energy splitting and sum rule of isospin doublets. It is shown that the splitting of GDR isospin doublets deviates from the systematic values when nucleus is away from the β-stability line. The ratio of $T_<$ and $T_>$ EWSR values are consistently larger than the systematic values, and it is noticed that the calculated EWSR ratio over the systematic ratio increases with increasing isospin almost linearly. How this linearity is explained poses a very interesting question to nuclear theorists.

The EWSRs of the PDRs in odd-Z nitrogen were compared with those in the neighboring even-Z carbon and oxygen. The exhaustion of the EWSRs summing up to 15 MeV shows a decreasing tendency with increasing Z for neutron-rich nuclei with the same $N - Z$, which is consistent with tendency of the cluster sum rule over the classical sum rule. Thus it is also consistent with the suggestion that the PDRs in the light-mass neutron-rich nuclei are caused by the soft dipole mode.

The photoabsorption cross sections of the nitrogen isotopes were calculated from the electric dipole strengths. To mend the enhancement of transition strengths, normalization factors were proposed for the 0–1$\hbar\omega$ and 2–3$\hbar\omega$ calculations. After the normalization, the shell model has well reproduced the experimental photoabsorption cross sections in ^{14,15}N, especially the detailed structure of resonances.

ACKNOWLEDGMENTS

The authors acknowledge the support from the NSF of China under Contracts No. 11205245, No. 11375266, No. 10975189, and No. 11405273.

[1] S. S. Dietrich and B. L. Berman, At. Data Nucl. Data Tables **38**, 199 (1988).
[2] E. Lipparini and S. Stringari, Phys. Rep. **175**, 103 (1989).
[3] B. L. Berman and S. C. Fultz, Rev. Mod. Phys. **47**, 713 (1975).
[4] A. V. D. Woude, Prog. Part. Nucl. Phys. **18**, 217 (1987).
[5] P. G. Hansen and B. Jonson, Europhys. Lett. **4**, 409 (1987).
[6] T. Kobayashi, Nucl. Phys. A **553**, 465 (1993).
[7] N. Paar, D. Vretenar, E. Khan, and G. Colò, Rep. Prog. Phys. **70**, 691 (2007).
[8] D. Savran, T. Aumann, and A. Zilges, Prog. Part. Nucl. Phys. **70**, 210 (2013).
[9] S. Goriely, Phys. Lett. B **436**, 10 (1998).
[10] J. Chambers, E. Zaremba, J. P. Adams, and B. Castel, Phys. Rev. C **50**, R2671 (1994).
[11] I. Hamamoto, H. Sagawa, and X. Z. Zhang, Phys. Rev. C **57**, R1064 (1998).
[12] D. Vretenar, N. Paar, P. Ring, and G. A. Lalazissis, Phys. Rev. C **63**, 047301 (2001).
[13] N. Paar, P. Ring, T. Nikšić, and D. Vretenar, Phys. Rev. C **67**, 034312 (2003).
[14] L.-G. Cao and Z.-Y. Ma, Phys. Rev. C **71**, 034305 (2005).
[15] J. Liang, L.-G. Cao, and Z.-Y. Ma, Phys. Rev. C **75**, 054320 (2007).
[16] E. Litvinova, P. Ring, and V. Tselyaev, Phys. Rev. C **78**, 014312 (2008).
[17] J. Daoutidis and P. Ring, Phys. Rev. C **80**, 024309 (2009).
[18] M. Martini, S. Péru, and M. Dupuis, Phys. Rev. C **83**, 034309 (2011).
[19] G. Colò and P. F. Bortignon, Nucl. Phys. A **696**, 427 (2001).
[20] M. Matsuo, Nucl. Phys. A **696**, 371 (2001).
[21] D. Vretenar, N. Paar, P. Ring, and G. A. Lalazissis, Nucl. Phys. A **692**, 496 (2001).
[22] A. Leistenschneider *et al.*, Phys. Rev. Lett. **86**, 5442 (2001).
[23] H.-L. Ma, B.-G. Dong, Y.-L. Yan, H.-Q. Zhang, and X.-Z. Zhang, Phys. Rev. C **85**, 044307 (2012).
[24] D. Sarchi, P. Bortignon, and G. Colò, Phys. Lett. B **601**, 27 (2004).
[25] I. Hamamoto and X. Z. Zhang, Phys. Rev. C **58**, 3388 (1998).
[26] C. J. Lin, X. Z. Zhang, R. Zhang, Z. H. Liu, and H. Q. Zhang, Phys. Rev. C **76**, 044321 (2007).

[27] T. Nakamura *et al.*, Phys. Lett. B **331**, 296 (1994).
[28] T. Nakamura *et al.*, Phys. Rev. Lett. **83**, 1112 (1999).
[29] H. R. Kissener, R. A. Eramzhian, and H. U. Jäger, Nucl. Phys. A **207**, 78 (1973).
[30] H. Sagawa and T. Suzuki, Phys. Rev. C **59**, 3116 (1999).
[31] T. Suzuki, H. Sagawa, and K. Hagino, Phys. Rev. C **68**, 014317 (2003).
[32] E. K. Warburton and B. A. Brown, Phys. Rev. C **46**, 923 (1992).
[33] B. A. Brown and W. D. M. Rae, MSU-NSCL Report, 2007 (unpublished).
[34] D. Gloeckner and R. Lawson, Phys. Lett. B **53**, 313 (1974).
[35] R. D. Lawson, *Theory of the Nuclear Shell Model* (Clarendon Press, New York, 1980).
[36] B. A. Brown, Lecture Notes in Nuclear Structure Physics, 2005 (unpublished).
[37] C. S. Sumithrarachchi, D. W. Anthony, P. A. Lofy, and D. J. Morrissey, Phys. Rev. C **74**, 024322 (2006).
[38] B. K. Agrawal, S. Shlomo, and V. K. Au, Phys. Rev. C **72**, 014310 (2005).
[39] M. Dutra *et al.*, Phys. Rev. C **85**, 035201 (2012).
[40] A. Ozawa, T. Suzuki, and I. Tanihata, Nucl. Phys. A **693**, 32 (2001).
[41] E. Liatard *et al.*, Europhys. Lett. **13**, 401 (1990).
[42] A. Bohr and B. R. Mottelson, *Nuclear Structure*, Vol. 2 (Benjamin, Massachusetts, 1975).
[43] R. A. Eramzhyan, B. S. Ishkhanov, I. M. Kapitonov, and V. G. Neudatchin, Phys. Rep. **136**, 229 (1986).
[44] Y. Utsuno, N. Shimizu, T. Otsuka, S. Ebata, and M. Honma, Prog. Nucl. Energy **82**, 102 (2015).
[45] G. Co, V. De Donno, C. Maieron, M. Anguiano, and A. M. Lallena, Phys. Rev. C **80**, 014308 (2009).
[46] W. D. Myers and W. J. Swiatecki, Ann. Phys. **84**, 186 (1974).
[47] R. O. Akyüz and S. Fallieros, Phys. Rev. Lett. **27**, 1016 (1971).
[48] S. Fallieros and B. Goulard, Nucl. Phys. A **147**, 593 (1970).
[49] D. Gambacurta, M. Grasso, and F. Catara, Phys. Rev. C **84**, 034301 (2011).
[50] P. Papakonstantinou, H. Hergert, V. Ponomarev, and R. Roth, Phys. Lett. B **709**, 270 (2012).
[51] V. Derya *et al.*, Phys. Lett. B **730**, 288 (2014).
[52] N. Paar, T. Niki, D. Vretenar, and P. Ring, Phys. Lett. B **606**, 288 (2005).
[53] Y. Alhassid, M. Gai, and G. F. Bertsch, Phys. Rev. Lett. **49**, 1482 (1982).
[54] B. Ishkhanov *et al.*, R MSU-INP-2002-27/711, 2002 (unpublished); also see the CDFE database, http://cdfe.sinp.msu.ru, SUBENT: M0648001.
[55] A. D. Bates, R. P. Rassool, E. A. Milne, M. N. Thompson, and K. G. McNeill, Phys. Rev. C **40**, 506 (1989).